2014/10/15
Head Id: 262133
Archive Id: 264024M
Archive Date: 2014/09/27
Archive Tag: trunk

# Search for natural SUSY using razor variables in events with b-tagged jets in pp collisions at $\sqrt{s} = 8$ TeV

The CMS Collaboration



## Abstract

An inclusive search for supersymmetry in events with at least one bottom-quark jet is carried out on proton-proton collision data collected by the CMS experiment in 2012 at a center-of-mass energy of 8 TeV. The dataset size corresponds to an integrated luminosity of 19.3 $fb^{-1}$. The event distribution in the plane defined by the razor variables $R^2$ and $M_R$ is studied in events with and without leptons, searching for a peaking signal on top of a smoothly falling standard model background. The data are consistent with the expected background, modeled by a template function. The exclusion limit on the supersymmetric particle masses at 95% confidence level is derived in several simplified supersymmetric scenarios with varying branching ratio choices. By combining the likelihoods of the razor search in events without leptons and an exclusive single-lepton search, an improved bound on the top-squark mass is obtained. For a lightest supersymmetric particle mass of 100 GeV and depending on (independent of) the branching ratio choice, the pair production of gluinos and top squarks is excluded for gluino masses up to 1375 GeV (1275 GeV) and for squark masses up to 750 GeV (675 GeV).

# 1 Introduction

Supersymmetry (SUSY) is a proposed symmetry of nature, which introduces a bosonic partner for every fermion and a fermionic partner for every boson [1–9]. Supersymmetric extensions of the standard model that include a stable new particle at the electroweak scale are well-motivated because they may explain the origin of dark matter and allow for the grand unification of the strong and the electroweak forces. The discovery of the Higgs boson [10, 11] at the Large Hadron Collider (LHC) has renewed interest in natural SUSY models, which minimize the fine-tuning associated with the observed value of the Higgs boson mass and its radiative corrections in the standard model. In the typical spectrum of these models, the lightest chargino and the lightest neutralino are higgsino-like with almost degenerate masses, the bottom and top squarks are the lightest squarks, and the gluino is heavier than these particles but potentially accessible at the LHC [12]. Previous searches for SUSY at the LHC at a center-of-mass energy of $\sqrt{s} = 7$ TeV have excluded gluino masses up to 1.1 TeV and squark masses up to 800 GeV [13–15].

We discuss here an inclusive search for squarks and gluinos in the context of natural SUSY spectra, performed on events with two or more jets, at least one of which is identified as originating from a bottom quark (jet b-tagging). The search is carried out on the data collected by the Compact Muon Solenoid (CMS) Collaboration in proton-proton collisions at $\sqrt{s} = 8$ TeV in 2012, corresponding to an integrated luminosity of 19.3 $\text{fb}^{-1}$. We exploit the razor kinematic variables $R^2$ and $M_R$ [16, 17] to search for a broadly peaking signal on the smoothly falling standard model (SM) background. The analysis is performed in several disjoint datasets (referred to as *boxes*), differing in the lepton and the jet multiplicity. Each box with less than two identified leptons is analyzed in exclusive b-tagged jet multiplicity bins, to maximize the sensitivity to direct and cascade production of third generation squarks. This search extends a previous analysis by CMS, performed with the same technique on the data collected at a center-of-mass energy of 7 TeV [18, 19]. The razor variables have also been used by the ATLAS Collaboration for a multi-channel search for SUSY at a center-of-mass energy of 7 TeV [20] and an exclusive search in events with two leptons at 8 TeV [21].

For a given box and b-tagged jet multiplicity, the background shape is modeled in two rectangular regions of the ($M_R$, $R^2$) plane (sidebands), designed so that the possible signal contamination has a negligible impact. The background shape is then extrapolated to the rest of the ($M_R$, $R^2$) plane (signal-sensitive region) to derive the SM background prediction. We observe a good agreement between the predicted background and the data yields in the signal-sensitive regions. This result is then interpreted in the context of several SUSY simplified models [22–26] by performing a hypothesis test between the background-only shape and the signal-plus-background shape using the data in the two sidebands and the signal-sensitive region simultaneously [27].

An improved bound on top-squark pair production is obtained by combining the all-hadronic razor boxes with a dedicated exclusive top-squark search in the events with one lepton [28]. For the exclusive single-lepton search, only the region with the best expected cross section upper limit contributes to the combination. For the search with razor variables, only the purely hadronic boxes are considered. An explicit lepton veto is applied so that the results of the two searches are mutually exclusive. As neither search observes an excess above the estimated background, the results are interpreted here as limits on the colored sparticle production.

This paper is organized as follows. The CMS detector is briefly described in Section 2. The event selection and razor variables are described in Sections 3 and 4, respectively. The statistical model used to describe the SM backgrounds as well as the comparisons between predicted

and observed yields in the search regions are detailed in Section 5. The constraints on the production of gluinos and top squarks are obtained in the context of simplified natural SUSY models [12], whose spectra are described in Section 6, followed by a summary of the limit setting procedure in Section 7. The interpretations and the conclusions are then presented in Sections 8 and 9, respectively.

# 2 The CMS detector

The central feature of the CMS particle detector [29] is a superconducting solenoid of 6 m internal diameter, providing a magnetic field of 3.8 T. Within the superconducting solenoid volume are a silicon pixel and a silicon strip tracker, a lead tungstate crystal electromagnetic calorimeter (ECAL), and a brass/scintillator hadron calorimeter, each composed of a barrel and two endcap sections. Muons are measured in gas-ionization detectors embedded in the magnet steel flux-return yoke outside the solenoid. Extensive forward calorimetry complements the coverage provided by the barrel and endcap detectors. Events are detected by a two-layer trigger system, based on a hardware filter (L1), followed by a software-based High Level Trigger (HLT).

CMS uses a coordinate system with the $x$-axis pointing towards the center of the LHC, the $y$-axis pointing up (perpendicular to the LHC plane), and the $z$-axis along the counterclockwise beam direction. The azimuthal angle $\phi$ is measured with respect to the $x$-axis in the $xy$ plane and the polar angle $\theta$ is defined with respect to the $z$-axis. The pseudorapidity is $\eta = -\ln[\tan(\theta/2)]$.

# 3 Event selection

The inclusive razor analysis is performed on the events detected by a set of dedicated triggers in the HLT, consisting of a loose selection on $M_R$ and $R^2$. The events are also required to satisfy a L1 requirement of two jets in the central part of the detector.

Given the nature of the background estimation in this search (modeling the SM backgrounds as a smooth function), razor-specific triggers are necessary to ensure the SM background shapes in the razor variables are not distorted by performing a selection with only partially correlated variables. The razor triggers reject the majority of the SM background at low $R^2$ and low $M_R$ while keeping the events in the signal-sensitive regions of the ($M_R$, $R^2$) plane. Two kinds of triggers are used: i) the hadronic razor trigger, selecting events with at least two jets having $p_T > 64\,\text{GeV}$ by applying threshold requirements on $R^2$, $M_R$, and their product; ii) the muon or electron razor triggers, combining looser requirements on $R^2$, $M_R$, and their product, with the requirement of at least one isolated muon or electron with transverse momentum $p_T > 12\,\text{GeV}$. The trigger efficiency, studied using a dedicated prescaled trigger, is measured to be $(95 \pm 5)\%$ and independent of $R^2$ and $M_R$ for the events selected by the baseline requirements described in Section 4.

Events are selected with at least one high-quality reconstructed interaction vertex. If more than one vertex is found, the one with the highest associated sum of tracks $p_T^2$ is used as the interaction point for event reconstruction. Detector- and beam-related cleaning algorithms are used to remove events with detector noise that would fake event topologies with high energy and large transverse momentum imbalance.

The analysis uses a global event description based on the CMS particle flow (PF) algorithm [30, 31]. Individual particles (PF candidates) are reconstructed combining the information of the

inner tracker, the calorimeters, and the muon system. Five categories of PF candidates are defined: muons, electrons, photons (including their conversions to $e^+e^-$ pairs), charged hadrons, and neutral hadrons. The contamination from other proton-proton collisions in the same or in neighbor bunch crossings is reduced by discarding the charged PF candidates not compatible with the interaction point. When computing lepton isolation and jet energy, the corresponding contamination from neutral particles is subtracted on average by applying an event-by-event correction based on the jet-area method [32–34].

A "tight" lepton identification is used for muons and electrons, consisting of isolation and track reconstruction quality. For electrons, the shape of the energy deposit in ECAL is used to further reduce the contamination from hadrons. For events with one identified tight lepton, additional muons or electrons are identified through a "loose" lepton selection, characterized by a relaxed isolation requirement.

Jets are reconstructed by clustering the PF candidates with the FastJet [35] implementation of the anti-$k_T$ [36] algorithm with the jet size set to $R = 0.5$. We select events containing at least two jets with $p_T > 80$ GeV and $|\eta| < 2.4$, a tighter version of the L1 filter criterion. The $p_T$ imbalance in the event, $\vec{E}_T^{miss}$, is the negative of the sum of the $\vec{p}_T$ of the PF candidates in the event. For each event, the $\vec{E}_T^{miss}$ and the four-momenta of all the jets with $p_T > 40$ GeV and $|\eta| < 2.4$ are used to compute the razor variables, as described in Section 4.

The medium working point of the combined secondary vertex algorithm [37] is used for jet b-tagging. The b-tagging efficiency and mistag probability are measured on data control samples, as a function of the jet $p_T$ and $\eta$. Correction factors are derived for Monte Carlo (MC) simulations, comparing the b-tagging efficiency and mistag rate on multijet and $t\bar{t}$ data samples [37] to the corresponding MC values.

Events without at least one b-tagged jet are discarded, a criterion motivated by the expectation of a light top or bottom squark accessible at LHC from naturalness considerations. A tighter requirement ($\geq$ 2 b-tagged jets) is imposed on events without an identified tight lepton and less than four jets to reduce the $Z(\rightarrow \nu\bar{\nu})$+jets background to a negligible level.

The selection for the exclusive single-lepton search is described in [28].

# 4 Razor variables and box definition

The razor variables $M_R$ and $R^2$ are defined to describe the two-jet topology resulting from the production of two squarks, each decaying to a quark and the lightest SUSY particle (LSP), assumed to be a stable neutralino $\tilde{\chi}_1^0$. The four-momenta of the two jets are used to compute $M_R$ and $M_T^R$, defined as

$$M_R \equiv \sqrt{(|\vec{p}_{j_1}| + |\vec{p}_{j_2}|)^2 - (p_z^{j_1} + p_z^{j_2})^2}\,, \tag{1}$$

$$M_T^R \equiv \sqrt{\frac{E_T^{miss}(p_T^{j_1} + p_T^{j_2}) - \vec{E}_T^{miss}\cdot(\vec{p}_T^{j_1} + \vec{p}_T^{j_2})}{2}}\,, \tag{2}$$

where $\vec{p}_{j_i}$, $\vec{p}_T^{j_i}$, and $p_z^{j_i}$ are the momentum of the ith-jet, its transverse component, its longitudinal component, respectively, while $E_T^{miss}$ and $p_T^{j_i}$ are the magnitude of $\vec{E}_T^{miss}$ and $\vec{p}_T^{j_i}$, respectively. While $M_T^R$ quantifies the transverse momentum imbalance, $M_R$ estimates the energy scale in the event. The razor dimensionless ratio is defined as

$$R \equiv \frac{M_T^R}{M_R}\,. \tag{3}$$

In this search, we consider events with two or more jets. Each event is reduced to a two-jet topology by clustering the selected physics objects (jets and leptons) into two "megajets" [17–19]. The megajets are defined by dividing the reconstructed jets of each event into two partitions. Each partition contains at least one jet. The megajet four-momenta are defined as the sum of the four-momenta of the assigned jets. Of all the possible combinations, we select the one that minimizes the sum of the invariant masses of the two megajets. The box definitions are given in Table 1. In the table, boxes are ordered from the first box to be filled. Each event is assigned to the first box whose requirements it satisfies to ensure no event is assigned to two different boxes.

The events in the single-lepton and two-lepton boxes are detected by the electron and muon razor triggers. The remaining boxes, generically referred to as "hadronic" boxes, include events detected by the hadronic razor trigger.

In the two-lepton boxes, the ($M_R$, $R^2$) data distribution of events with at least one b-tagged jet is studied. For the other boxes, the data are binned according to the b-tagged jet multiplicity: 1b-tag, 2b-tag, and $\geq$ 3b-tag.

Table 1: Kinematic and multiplicity requirements defining the nine razor boxes. Boxes are listed in order of event filling priority. The ranking is introduced to unambiguously associate an event to the first box it fills.

| Requirements | | | | |
|---|---|---|---|---|
| Box | lepton | b-tag | kinematic | jet |
| Two-Lepton Boxes | | | | |
| MuEle | $\geq$ 1 tight electron and $\geq$ 1 loose muon | $\geq$ 1 b-tag | ($M_R > 300$ GeV and $R^2 > 0.15$) and ($M_R > 350$ GeV or $R^2 > 0.2$) | $\geq$ 2 jets |
| MuMu | $\geq$ 1 tight muon and $\geq$ 1 loose muon | $\geq$ 1 b-tag | ($M_R > 300$ GeV and $R^2 > 0.15$) and ($M_R > 350$ GeV or $R^2 > 0.2$) | $\geq$ 2 jets |
| EleEle | $\geq$ 1 tight electron and $\geq$ 1 loose electron | $\geq$ 1 b-tag | ($M_R > 300$ GeV and $R^2 > 0.15$) and ($M_R > 350$ GeV or $R^2 > 0.2$) | $\geq$ 2 jets |
| Single Lepton Boxes | | | | |
| MuMultiJet | $\geq$ 1 tight muon | $\geq$ 1 b-tag | ($M_R > 300$ GeV and $R^2 > 0.15$) and ($M_R > 350$ GeV or $R^2 > 0.2$) | $\geq$ 4 jets |
| MuJet | $\geq$ 1 tight muon | $\geq$ 1 b-tag | ($M_R > 300$ GeV and $R^2 > 0.15$) and ($M_R > 350$ GeV or $R^2 > 0.2$) | 2 or 3 jets |
| EleMultiJet | $\geq$ 1 tight electron | $\geq$ 1 b-tag | ($M_R > 300$ GeV and $R^2 > 0.15$) and ($M_R > 350$ GeV or $R^2 > 0.2$) | $\geq$ 4 jets |
| EleJet | $\geq$ 1 tight electron | $\geq$ 1 b-tag | ($M_R > 300$ GeV and $R^2 > 0.15$) and ($M_R > 350$ GeV or $R^2 > 0.2$) | 2 or 3 jets |
| Hadronic Boxes | | | | |
| MultiJet | none | $\geq$ 1 b-tag | ($M_R > 400$ GeV and $R^2 > 0.25$) and ($M_R > 450$ GeV or $R^2 > 0.3$) | $\geq$ 4 jets |
| 2b-tagged jet | none | $\geq$ 2 b-tag | ($M_R > 400$ GeV and $R^2 > 0.25$) and ($M_R > 450$ GeV or $R^2 > 0.3$) | 2 or 3 jets |

A baseline kinematic requirement is applied to define the region in which we search for a signal:

- $M_R > 400$ GeV and $R^2 > 0.25$ for the hadronic boxes,
- $M_R > 300$ GeV and $R^2 > 0.15$ for the other boxes.

The tighter baseline selection for the hadronic boxes is a consequence of the tighter threshold used for the hadronic razor trigger. The kinematic plane defined by the baseline selection is

divided into three regions (see Fig. 1):

- **Low $M_R$ sideband**: $400 < M_R < 550$ GeV and $R^2 > 0.30$ for the hadronic boxes; $300 < M_R < 450$ GeV and $R^2 > 0.20$ for the other boxes.
- **Low $R^2$ sideband**: $M_R > 450$ GeV and $0.25 < R^2 < 0.30$ for the hadronic boxes; $M_R > 350$ GeV and $0.15 < R^2 < 0.20$ for the other boxes.
- **Signal-sensitive region**: $M_R > 550$ GeV and $R^2 > 0.30$ for the hadronic boxes; $M_R > 450$ GeV and $R^2 > 0.20$ for the other boxes.

The bottom left corner of the razor plane, not included in any of the three regions, is excluded from the analysis. Given this selection, the multijet background from quantum chromodynamic processes is reduced to a negligible level due to the fact that these processes are typically balanced in the transverse plane and thus are peaking at zero in $R^2$ and exponentially suppressed above zero [18, 19].

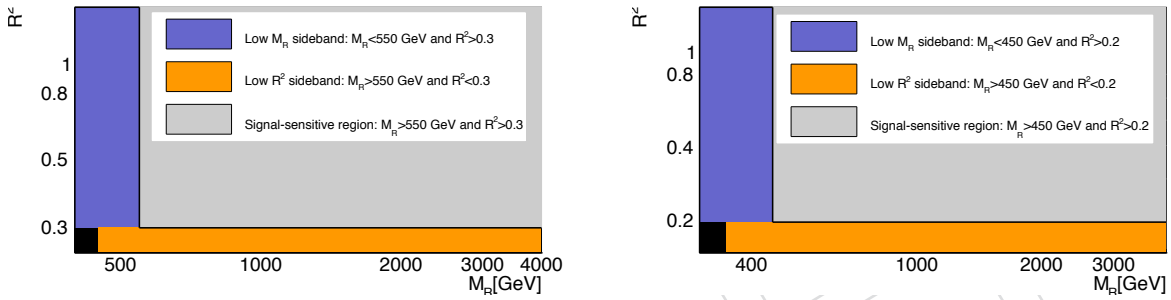


(a) (b)

Figure 1: Definition of the sideband and the signal-sensitive regions used in the analysis, for (a) the hadronic boxes and (b) the other boxes.

## 5 Modeling the standard model backgrounds

Under the hypothesis of no contribution from new physics processes, the event distribution in the ($M_R$, $R^2$) plane can be described by the sum of the weak vector boson plus jets production (V+jets where V = W, Z) and the top quark-antiquark and the top single-quark production, generically referred to as the $t\bar{t}$ contribution.

We study each of these processes using MC samples, generated with the MADGRAPH V5 simulation [38, 39]. Parton shower and hadronization effects are included by matching events to the PYTHIA V6 simulation [40] using the MLM algorithm [41]. The events are processed by a GEANT-based [42] description of the CMS apparatus to include detector effects.

Once normalized to the next-to-leading order (NLO) inclusive cross section and the integrated luminosity, the absolute yield of the V+jets contribution satisfying the event selection is found to be negligible in all of the two-lepton boxes. In the remaining boxes, its contribution to the total SM background is found to be approximately 25%. The contribution of V+jets in the $\geq$ 2b-tag and the $\geq$ 4jet sample is found to be negligible.

Based on the study of the data collected at $\sqrt{s} = 7$ TeV and the corresponding MC samples [18, 19], the two-dimensional probability density function $P_{SM}(M_R, R^2)$ of each SM process is found to be well described by the template function:

$$f(M_R, R^2) = [b(M_R - M_R^0)^{1/n}(R^2 - R_0^2)^{1/n} - 1]e^{-bn(M_R - M_R^0)^{1/n}(R^2 - R_0^2)^{1/n}}. \quad (4)$$

where $b$, $n$, $M_R^0$, and $R_0^2$ are free parameters of the background model. For $n = 1$, this function recovers the two-dimensional exponential function used for previous studies [18, 19]. The shape of the template function is determined through a ROOFIT-based extended and unbinned maximum likelihood (ML) fit to the data [43]. The template function is found to adequately describe the standard model background in each of the boxes, for each b-tagged jet multiplicity.

The SM background-only likelihood function for the two-lepton boxes is written as:

$$\mathcal{L}(\text{data}|\Theta) = \frac{e^{-N_{SM}}}{N!} \prod_{i=1}^{N} N_{SM} P_{SM}(M_{R(i)}, {R^2}_{(i)}) \,, \tag{5}$$

where $P_{SM}(M_R, R^2)$ is the template function in Eq. (4) normalized to unity, $\Theta$ is the set of background shape and normalization parameters, and the product runs over the N events in that dataset. The same form of the likelihood is used for the other boxes, for each b-tagged jet multiplicity. The total likelihood in these boxes is computed as the product of the likelihood functions for each b-tagged jet multiplicity.

The fits are performed independently for each box and simultaneously across the b-tagged jet multiplicity bins. Common background shape parameters are used for the 2b-tag and $\geq$3b-tag bins, since no substantial difference between the two distributions is observed on high-statistics samples of the $t\bar{t}$ and the V+jets MC events. On the other hand, a difference is observed between 1b-tag and $\geq$ 2b-tag samples, due to the observed dependence of the b-tagging efficiency on the jet $p_T$. Consequently, the shape parameters for the 1b-tag are allowed to be different than the corresponding parameters for the $\geq$ 2b-tag bins. The background normalization parameters for each b-tagged jet multiplicity bins are also treated as independent parameters.

The background shape parameters are estimated from the events in the two sidebands (see Section 4). This shape is then used to derive a background prediction in the signal-sensitive region: an ensemble of background shape parameters is sampled from the covariance matrix returned by the fit. A pseudo-experiment output ("toy" dataset) is generated from each of these alternative shapes. For each bin of the signal-sensitive region, the distribution of the toy-by-toy predicted yields is compared to the observed yield in data in order to quantify the agreement between the background model and the observation. The agreement, quantified as a two-sided p-value, is then translated into the corresponding number of standard deviations for a normal distribution. The observed numbers of standard deviations in the two-lepton boxes are shown in Fig. 2, as a function of $M_R$ and $R^2$. Similar results for the one-lepton and hadronic boxes are shown in Figs. 3 and 4, respectively. Figures 5 to 8 illustrate the extrapolation of the fit results to the full ($M_R$, $R^2$) plane, projected on $R^2$ and $M_R$ and summed over the b-tagged jet multiplicity bins. No significant deviation is observed.

To demonstrate the discovery potential of this analysis, we apply the background-prediction procedure to a simulated signal-plus-background MC sample. Figure 9 shows the $M_R$ and $R^2$ distributions of the SM background events and of a sample of gluino-gluino production, with each gluino decaying to a $b\bar{b}$ pair and a LSP. The $\tilde{g}$ and LSP masses are set to 1325 GeV and 50 GeV, respectively. A signal-plus-background sample is obtained adding the two distributions in Fig. 9, assuming an integrated luminosity of 19.3 fb$^{-1}$ and a gluino-gluino production cross section of 0.02 pb. The agreement between the background prediction from the sideband fit and the yield of the signal-plus-background toy data is displayed in Fig. 10. The signal contamination in the sideband has a negligible impact on the determination of the background shape, while a disagreement is observed in the signal-sensitive region, characterized as an excess of events clustered around $M_R \approx 1300$ GeV. The excess would indicate the discovery of a signal, and the position of the excess along the $M_R$ axis would provide information about the

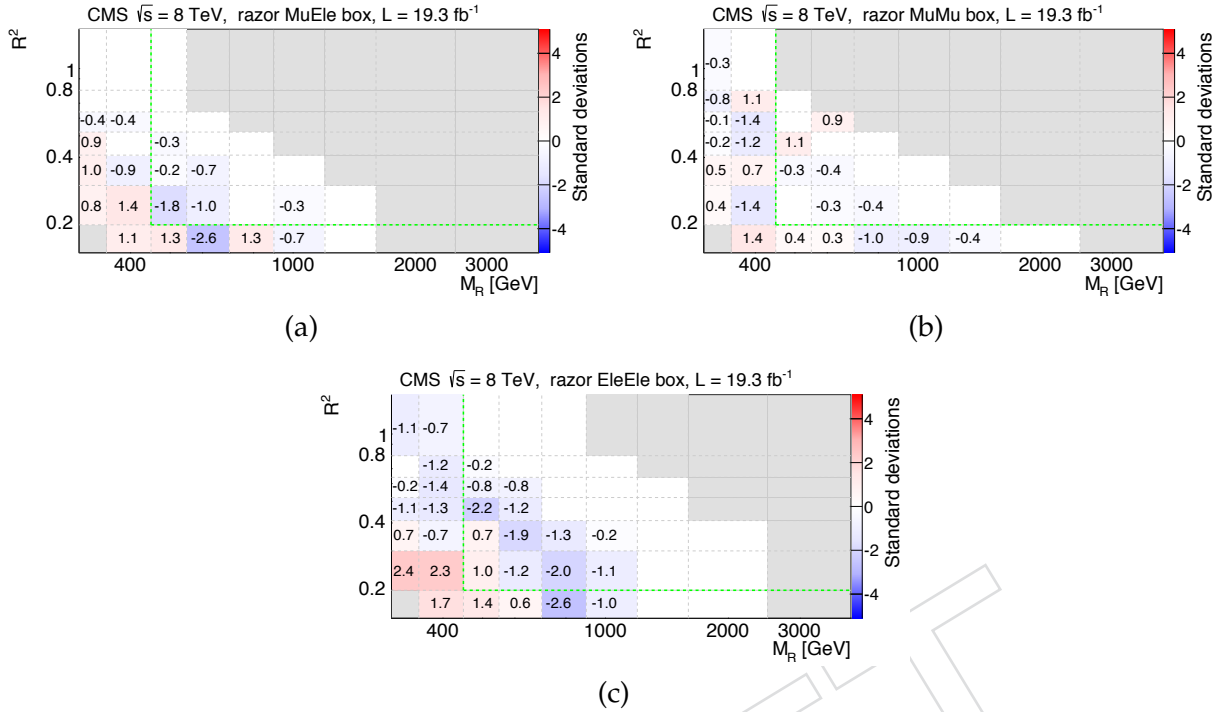


Figure 2: Comparison of the expected background and the observed yield in the (a) MuEle, (b) the MuMu, and (c) the EleEle boxes. A probability density function is derived for the bin-by-bin yield using toy experiments, sampled from the output of the corresponding sideband fit. A two sided p-value is computed comparing the observed yield to the distribution of background yield from toy experiments. The p-value is translated into the corresponding number of standard deviations, quoted in each bin and represented by the bin-filling color.

underlying SUSY spectrum.

# 6 Simplified Models

For this set of interpretations, a simplified natural SUSY spectrum is taken as a reference. The LSP is assumed to be a neutralino $\widetilde{\chi}_1^0$, 5 GeV lighter than a chargino $\widetilde{\chi}_1^\pm$. The chargino is forced to be the next-to-lightest SUSY particle (NLSP), with 100% branching fraction for the decay involving a virtual W (W$^*$), $\widetilde{\chi}_1^\pm \to \mathrm{W}^*\widetilde{\chi}_1^0$. Three other SUSY partners are assumed to be accessible at the LHC, namely the gluino and the lightest top and bottom squarks. The rest of the SUSY spectrum is assumed to be decoupled, with masses large enough to be inaccessible at the LHC. The SUSY partners composing this natural SUSY spectrum are summarized in Fig. 11, together with the possible decay modes.

In the context of this natural spectrum, five simplified models [22–26] are considered for gluino pair production:

- **T1bbbb**: pair-produced gluinos, each decaying with a 100% branching fraction to a pair of bottom quarks and the LSP.
- **T1tbbb**: pair-produced gluinos, each decaying with a 50% branching fraction to a pair of bottom quarks and the LSP or a top quark, a bottom quark, and the NLSP.
- **T1ttbb**: pair-produced gluinos, each decaying with a 50% branching fraction to a

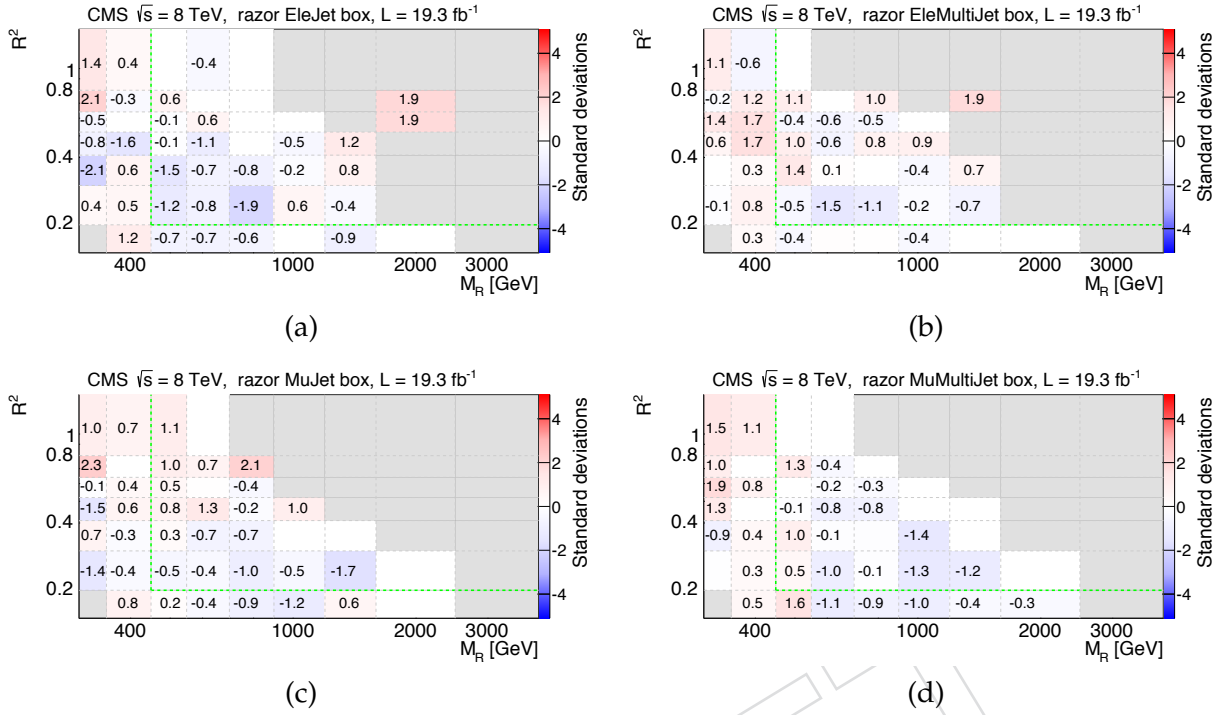


Figure 3: Comparison of the expected background and the observed yield in (a) the EleJet, (b) the EleMultiJet, (c) the MuJet, and (d) the MuMultiJet boxes. A detailed explanation is given in the caption of Fig. 2.

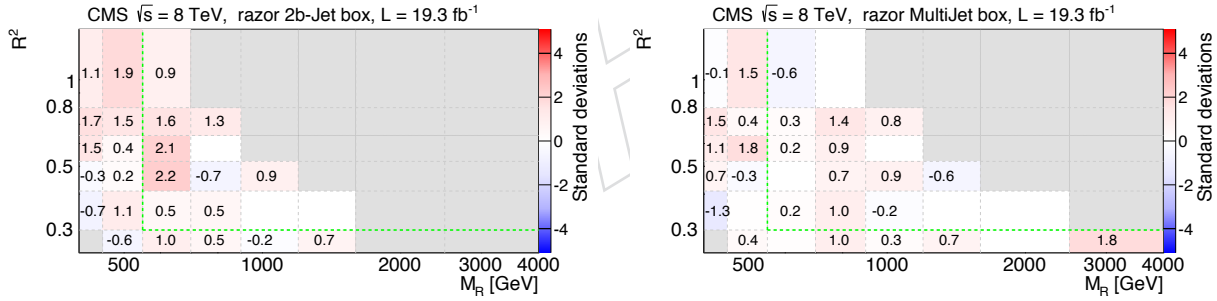


Figure 4: Comparison of the expected background and the observed yield in the 2b-tagged jet box (left) and the MultiJet box (right). A detailed explanation is given in the caption of Fig. 2.

pair of bottom quarks and the LSP or a pair of top quarks and the LSP.

- **T1tttb**: pair-produced gluinos, each decaying with a 50% branching fraction to a pair of top quarks and the LSP or a top quark, a bottom quark, and the NLSP.
- **T1tttt**: pair-produced gluinos, each decaying with a 100% branching fraction to a pair of top quarks and the LSP.

The corresponding Feynman diagrams are shown in Fig. 12.

In addition, the following three simplified models are considered for the production of top-squark pairs:

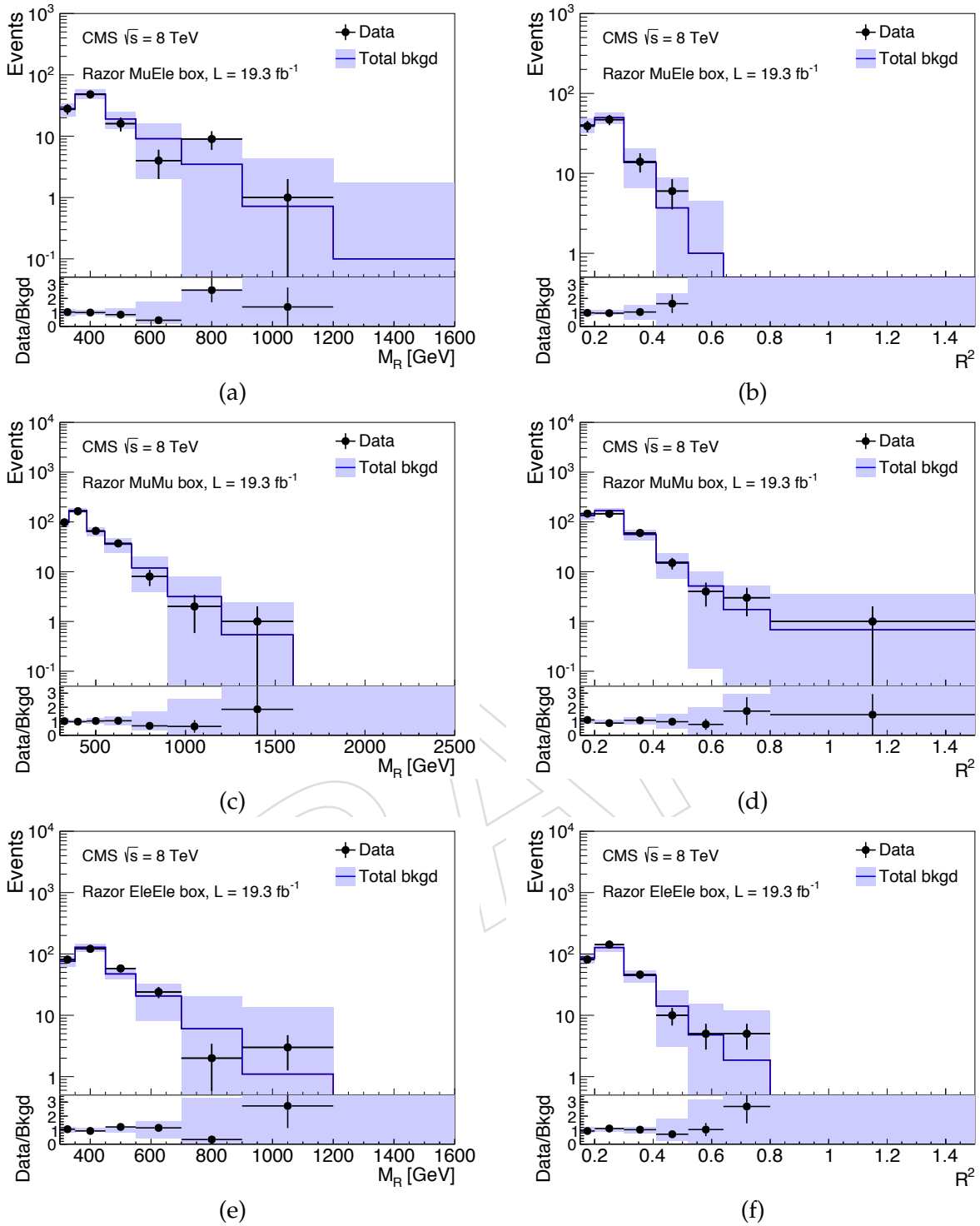


Figure 5: Projection of the sideband fit result in the (a-b) MuEle, (c-d) MuMu, and (e-f) EleEle boxes on $M_R$ and $R^2$, respectively. The fit is performed in the sideband regions and extrapolated to the signal-sensitive region. The solid line and the filled band represent the total background prediction and its uncertainty. The points and the band in the bottom panel represent the data-to-prediction ratio and the prediction uncertainty, respectively.

- **T2bW**$^*$: pair-produced top squarks, each decaying with a 100% branching fraction

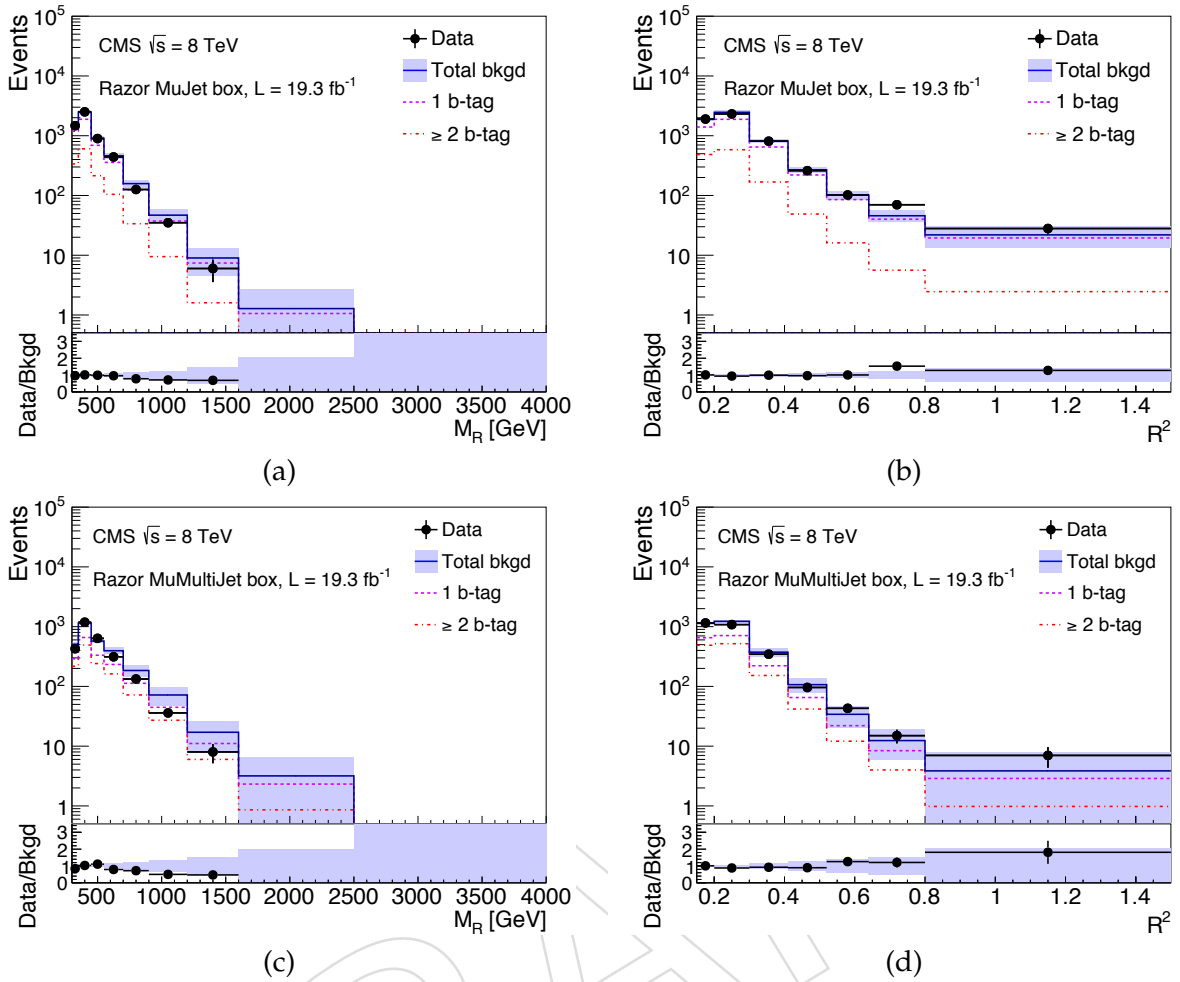


Figure 6: Projection of the sideband fit result in the MuJet box on (a) $M_R$ and (b) $R^2$, and of the sideband fit result in the MuMultiJet box on (c) $M_R$ and (d) $R^2$. The fit is performed in the sideband regions and extrapolated to the signal-sensitive region. The solid line and the filled band represent the total background prediction and its uncertainty. The dashed and dot-dashed lines represent the background shape for 1b-tag and $\geq$ 2b-tag events, respectively. The points and the band in the bottom panel represent the data-to-prediction ratio and the prediction uncertainty, respectively.

to a bottom quark and the NLSP.

- **T2tb**: pair-produced top squarks, each decaying with a 50% branching fraction to a top quark and the LSP or a bottom quark and the NLSP.
- **T2tt**: pair-produced top squarks, each decaying with a 100% branching fraction to a top quark and the LSP.

The corresponding Feynman diagrams are shown in Fig. 13.

We do not explicitly consider the corresponding simplified models for the bottom squark. Within the considered scenario, each top-squark decay to a chargino or neutralino is topologically similar to a bottom squark decay to neutralino or chargino, respectively. The correspondence is exact for small mass differences between the squarks and the chargino or neutralino, since in this case the visible decay products of the chargino decay are too soft to be detected.

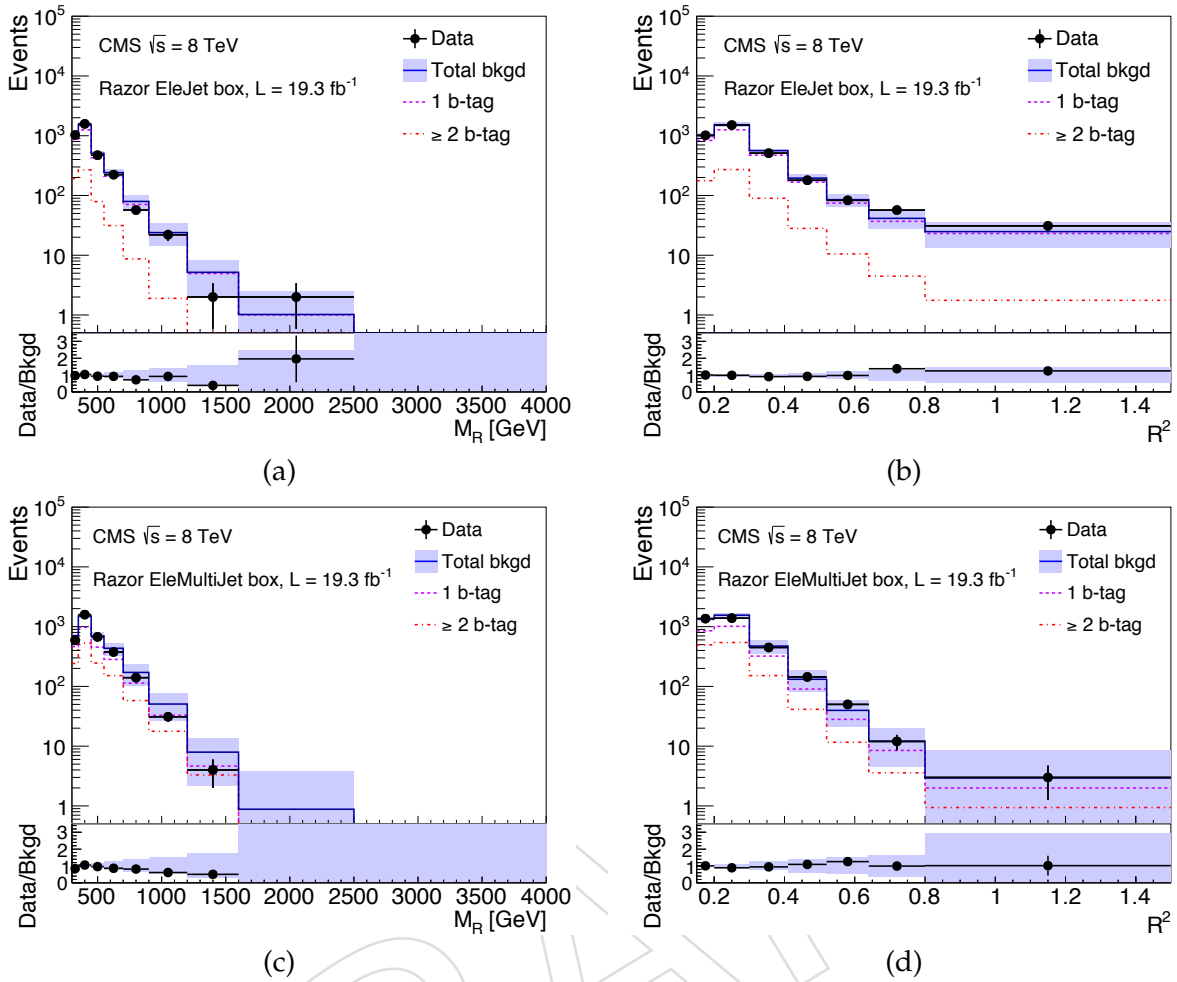


Figure 7: Projection of the sideband fit result in the EleJet box on (a) $M_R$ and (b) $R^2$, and projection of the sideband fit result in the EleMultiJet box on (c) $M_R$ and (d) $R^2$. A detailed explanation is given in the caption of Fig. 6.

On the other hand, for large mass differences the visible decay products of the chargino decay can be boosted to a large-enough momentum to be reconstructed as an additional jet or lepton. With respect to the models without the intermediate decay to charginos, this implies for the search with razor variables a migration of reconstructed events from the low-background 2b-Jet box to the high-background MultiJet box, and a consequent relatively weaker limit for the simplified model with decays to charginos. The exclusive single-lepton search is conservatively taken to only have sensitivity when both top squarks decay to a top quark and a neutralino.

Events for the eight simplified models are generated with the MADGRAPH V5 simulation [38, 39], in association with up to two partons. The SUSY particles are decayed in the PYTHIA V6 simulation code assuming a flat matrix element. The event is showered in PYTHIA V6 and matched to the matrix-element kinematic configuration using the MLM algorithm [41], before being processed through a fast simulation of the CMS detector [44]. The SUSY particle production cross sections are calculated to next-to-leading order (NLO) and next-to-leading-logarithm (NLL) accuracy [45–49], assuming the decoupling of the other SUSY partners. The NLO+NLL cross section and the associated theoretical uncertainty [50] are taken as a reference to derive the exclusion limit on the SUSY particle masses.

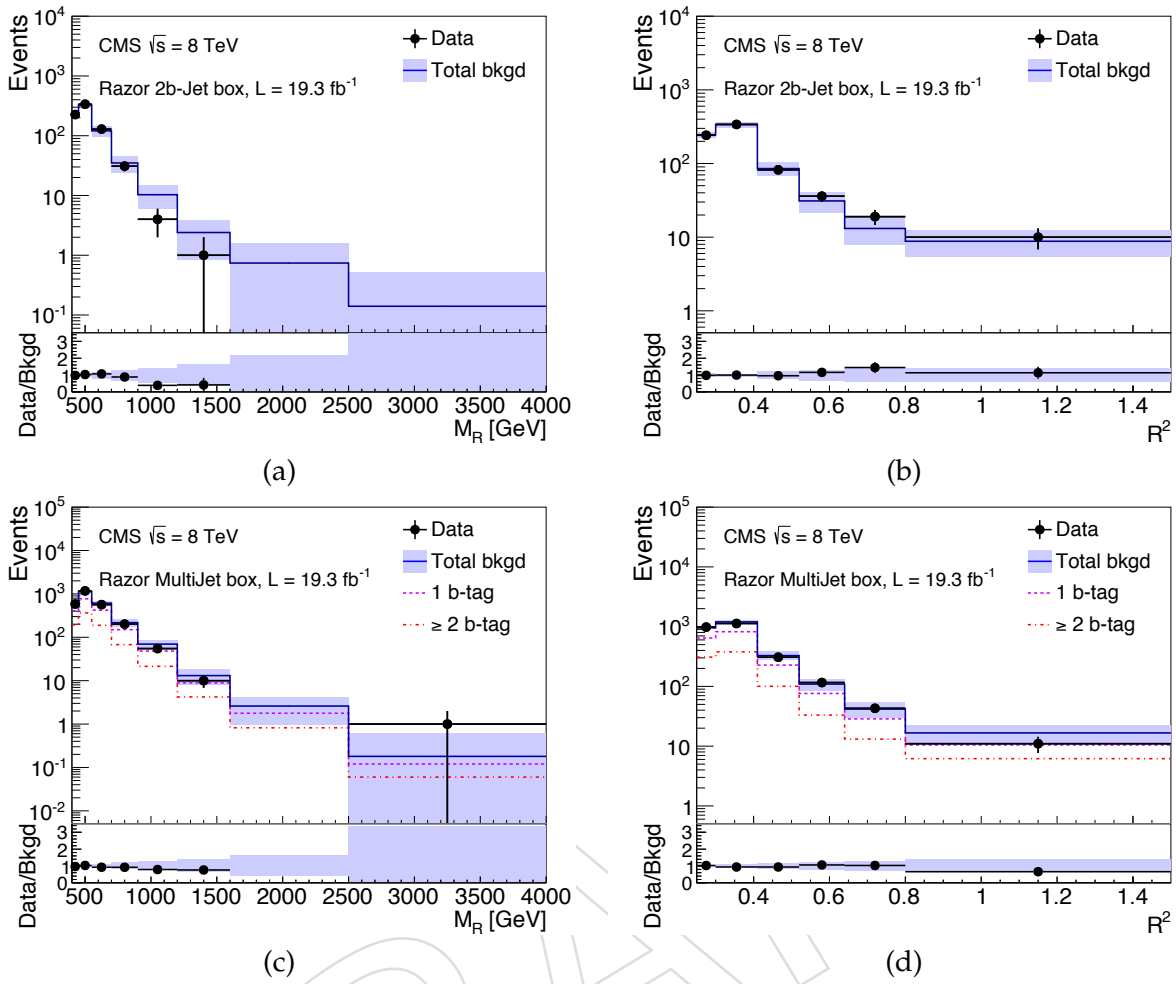


Figure 8: Projection of the sideband fit result in the 2b-tagged jet box on (a) $M_R$ and (b) $R^2$, and projection of the sideband fit result in the MultiJet box on (c) $M_R$ and (d) $R^2$. A detailed explanation is given in the caption of Fig. 6.

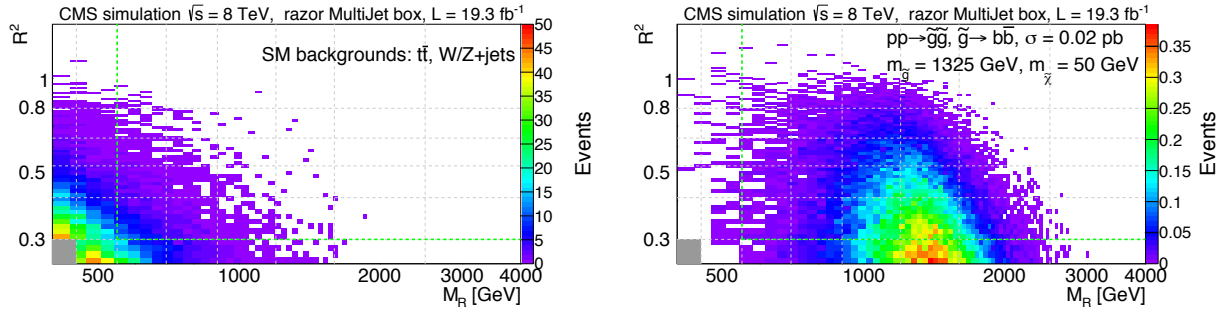


Figure 9: Distribution of (a) simulated standard model background events and (b) gluino-gluino events in the MultiJet box. Each $\tilde{g}$ is forced to decay to a $b\bar{b}$ pair and a $\tilde{\chi}_1^0$, assumed to be the stable LSP. The $\tilde{g}$ and $\tilde{\chi}_1^0$ masses are fixed to 1325 GeV and 50 GeV, respectively.

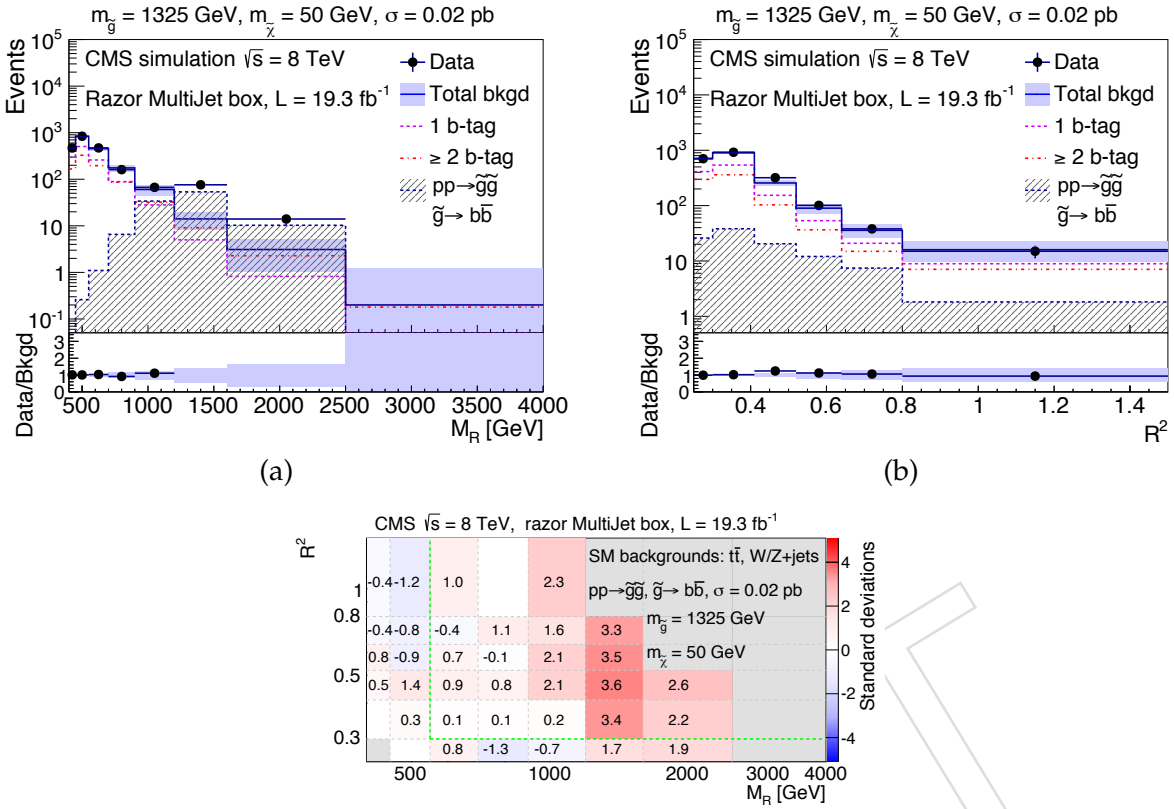


Figure 10: Result of the fit to the sideband events of a signal-plus-background MC sample, corresponding to the gluino model whose distribution is shown in Fig. 9. A gluino-gluino production cross section of 0.02 pb is assumed. The one-dimensional projections on (a) $M_R$ and (b) $R^2$ are shown, together with (c) the agreement between the observed yield and the prediction from the sideband fit as a function of $R^2$ and $M_R$. This agreement is quantified by the two-sided p-value using an ensemble of background-only toy datasets as described in Fig. 2.

# 7 The Limit Setting Procedure

We interpret the results of the searches by determining the 95% confidence level (CL) limit on SUSY models using the LHC $CL_s$ procedure [27], combining the likelihoods of different search boxes in a global likelihood. In contrast to the procedure described in Section 5, a binned likelihood is used to speed up the computation of the exclusion limit on the SUSY particle masses.

For the razor search boxes, the signal contribution is modeled by a template function, for a given signal hypothesis in a specific box and a given b-tagged jet multiplicity. The template function is normalized to the expected signal yield in each bin $\sigma \times L \times \epsilon^{\text{box}}_{\text{b-tag}}$, where $\sigma$ is the SUSY signal cross section, $L$ is the integrated luminosity corresponding to the dataset size, and $\epsilon^{\text{box}}_{\text{b-tag}}$ is the signal selection efficiency for a given box and, for single lepton and hadronic boxes, a given b-tagged jet multiplicity.

Each systematic effect is incorporated in the likelihood with a dedicated nuisance parameter, whose value is not known a priori but rather must be estimated from the data. The additional flexibility in the parametric model introduced by each nuisance parameter results in a loss

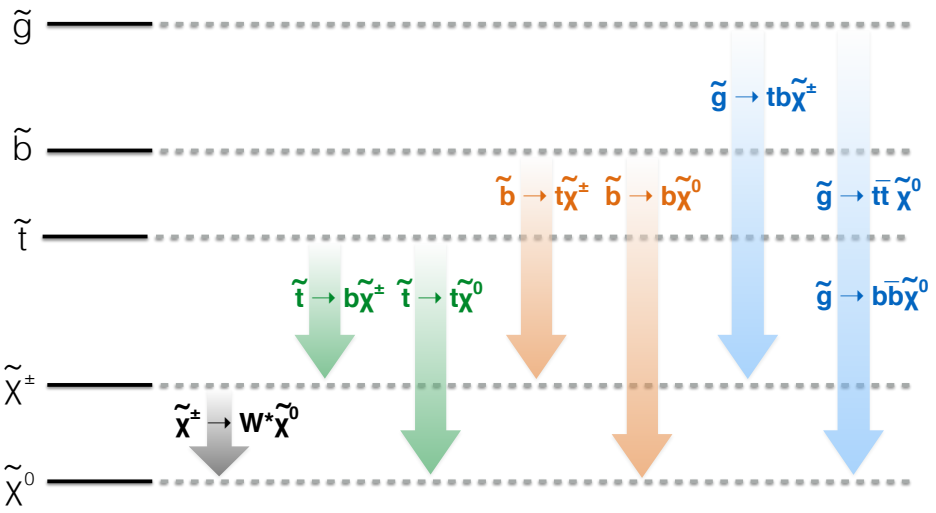


Figure 11: Simplified natural SUSY spectrum considered as a benchmark for result interpretations. The neutralino is forced to be the lightest SUSY particle. The difference in mass between the chargino and the neutralino is fixed at 5 GeV. Gluino and same-flavor squark pair production are considered in separate models, scanning the masses of the produced SUSY particle and the neutralino.

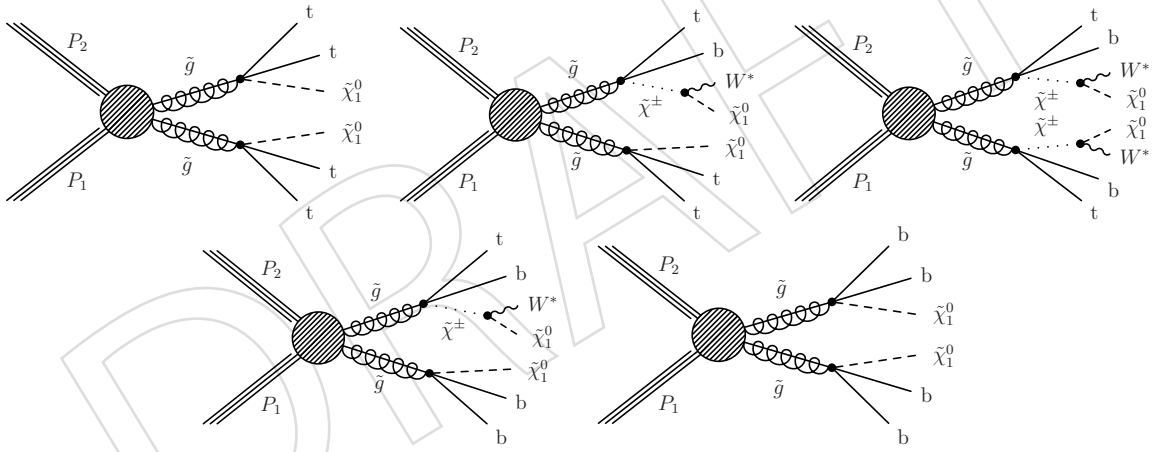

Figure 12: Diagrams displaying the event topologies of gluino pair production considered in this note.

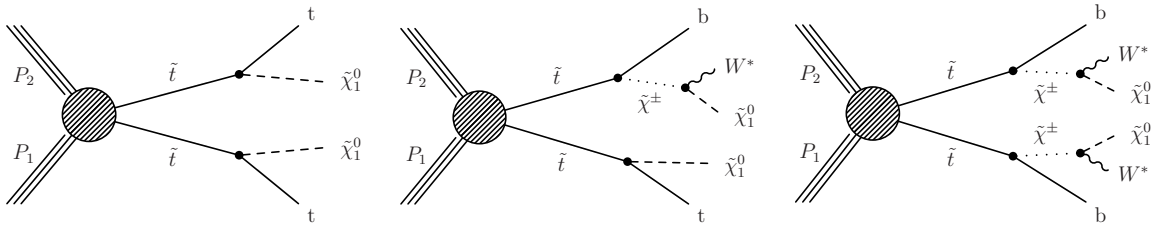

Figure 13: Diagrams displaying the event topologies of top-squark pair production considered in this note.

of sensitivity and adds an additional systematic uncertainty. The set of nuisance parameters may be divided into three distinct classes (though their statistical treatment is the same): those related to the signal normalization, those related to the signal shape, and those related to the background normalization and shape.

We consider the following systematic uncertainties associated with the signal normalization, the size of the uncertainty being indicated between parentheses for each of the categories stated below:

- integrated luminosity (2.6%),
- trigger efficiency (5%),
- electron and muon reconstruction and identification (3% per lepton), measured on an inclusive $Z \to \ell\ell$ sample as a function of the lepton $p_T$ and $\eta$ values.

In addition, four signal shape systematic uncertainties are considered, whose sizes vary with $R^2$, $M_R$, and the b-tagged jet multiplicity:

- The uncertainty in the jet b-tagging and mistagging efficiencies, evaluated for each ($M_R$, $R^2$) and b-tagged jet multiplicity bin. The uncertainty is quantified propagating the uncertainty in data-to-simulation scale factors [37],
- The uncertainty in the modeling of the parton density functions (PDF), evaluated bin-by-bin in the ($M_R$, $R^2$) plane for each box and b-tag multiplicity, following the PDF4LHC prescription [51–53]. The report recommends the use of the predictions and the respective 68% CL uncertainty bands from three different PDF sets to derive the final prediction (the mean of the three predictions) and the final uncertainty (the envelope of the three uncertainty bands) for the yield in one bin of the distribution of a generic observable.
- The uncertainty in the jet energy scale and resolution, evaluated from a set of data control samples and MC simulations,
- The uncertainty in the modeling of the associated jet production by the MADGRAPH simulation, studied on data samples of Z+jets and $t\bar{t}$ and parameterized as a MC-to-data scale factor as a function of the sum of the $\vec{p}_T$ of the two produced SUSY particles [28].

The impact of each of these uncertainties on the SUSY signal shape is taken into account by varying each effect by plus or minus one standard deviation to form the $\pm 1\sigma$ template distributions. Each effect is assigned a single nuisance parameter, which continuously interpolates between the nominal distribution and the $\pm 1\sigma$ template distributions.

The uncertainty on the knowledge of the background distributions is taken into account by maximizing the likelihood with respect to the background shape and normalization parameters using the data in the two sidebands and the signal-sensitive region. The background parameterization is able to accomodate several sources of systematic uncertainties defined below:

- dependence of the background shape on the b-tag multiplicity,
- dependence of the background shape on the lepton and jet multiplicities,
- deviation of the two-dimensional shape from an exponential falling distribution, through the background template function parameter $n$, which modifies the tail in $M_R$ and $R^2$
- shape bias induced by the dependence of b-tagging efficiency and mistag rate on the

jet $p_{\mathrm{T}}$,

- deviation of the b-tagging and mistagging efficiencies from the MC prediction, through independent normalization factors in each b-tagged jet multiplicity bin.

In order to analyze the global likelihood purely as a function of the parameter of interest: namely the SUSY signal cross section $\sigma$, the dependence of the likelihood on the nuisance parameters is removed by maximizing the likelihood with respect to all of the nuisance parameters. The test statistic is defined as

$$\tilde{q}_\sigma = -2\log\frac{\mathcal{L}(\text{data}|\sigma,\hat{\Theta}_\sigma)}{\mathcal{L}(\text{data}|\hat{\sigma},\hat{\Theta}_{\hat{\sigma}})} \tag{6}$$

where $\mathcal{L}$ refers to the global likelihood function, $\hat{\Theta}_\sigma$ is the set nuisance parameter values that maximize the likelihood evaluated at $\sigma$ (the hypothesized value), $\hat{\sigma}$ is the value of cross section that maximizes the likelihood in the range $0 < \hat{\sigma} \leq \sigma$, and "data" may refer to the actual experimental observation or pseudo-data (toys).

Each hypothesized value of $\sigma$ is associated with a confidence level value ($\mathrm{CL_s}$), defined as a ratio of probabilities,

$$\mathrm{CL_s} \equiv \frac{P(\tilde{q}_\sigma \geq \tilde{q}_\sigma^{\mathrm{obs}}|\text{signal+background})}{P(\tilde{q}_\sigma \geq \tilde{q}_\sigma^{\mathrm{obs}}|\text{background-only})} \tag{7}$$

where the numerator (denominator) is the probability that the test statistic is less than that observed in the data assuming the presence of both signal and background (only background). The 95% C.L. upper limit on the SUSY signal cross section (corresponding to the $\sigma$ value at which $\mathrm{CL_s} = 0.05$) is computed for each point of a given model's two-dimensional SUSY mass plane. The 95% C.L. mass exclusion contour is derived by intersecting this surface with the NLO+NLL cross section surface.

The combination of razor and exclusive single lepton searches is performed using the same procedure, taking into account the systematic uncertainties associated with the five following effects:

- the parton density functions
- the jet energy scale correction
- the integrated luminosity
- the b-jet tagging efficiency
- the associated jet production

The uncertainties on the background predictions are considered uncorrelated, being derived from independent data control samples with different techniques. We verified that the correlation model for the systematics has a negligible impact on the combination, since similar results are derived neglecting any correlation between the systematic uncertainties of the two searches.

# 8 Interpretation

The result of this search is interpreted in the context of the natural SUSY simplified models of gluino-gluino and squark-squark production described in Section 6.

## 8.1 Limits on gluino pair production

Derived limits for gluino-gluino production decaying to top and bottom quarks are shown in Figs. 14. A comparison of the simplified natural SUSY gluino-gluino exclusions, obtained for the different final state combinations of third generation quarks, is shown in Fig. 15. The limits corresponding to gluino-gluino topologies with mixed branching fractions lie within the band outlined by the T1bbbb and the T1tttt contours. As an example, gluino masses smaller than 1275 GeV for T1tttt and 1375 GeV for T1bbbb are excluded, depending on the gluino branching fractions, for a LSP mass of 100 GeV. For any LSP mass value, a larger number of top quarks in the decay topology corresponds to a weaker limit, mainly due to a reduced total signal efficiency with respect to the four-bottom-quark final state and a worse $M_R$ and $R^2$ resolution for events with higher jet multiplicity in the final state. Given this fact and the inclusive nature of the analysis, the T1tttt limit can be considered a conservative estimate of a branching-fraction-independent limit, generically valid for gluino-gluino production within the context of the simplified SUSY spectrum shown in Fig. 11.

## 8.2 Limits on top-squark pair production

Derived limits for squark-squark production are shown for the search with razor variables in Figure 16 and compared in Figure 17, while those for the exclusive single-lepton top-squark search were reported previously [28]. Similarly, as in the case of the gluino interpretation, the expected limit from the razor search improves as the number of top quarks in the decay topology decreases. For a LSP mass of 100 GeV, top-squark mass values larger than 375 GeV and smaller than 660 GeV are excluded in all three top-squark branching ratio scenarios considered in the razor search.

A stronger limit on top-squark pair production is derived combining the hadronic boxes of the razor search with the results of the exclusive single-lepton analysis. Figure 18 shows the combined result obtained for the scenario where the top squark only decays to top quark and the lightest neutralino. For a LSP mass of 100 GeV, the combination improves the constraint on the top-squark mass by approximately 70 GeV, from 680 GeV to 750 GeV. This result provides the best limit on these specific simplified models.

Figure 18 (c) shows a more generic limit on the top-squark mass. We consider two decay modes for the top squark, already introduced when discussing the simplified natural SUSY spectrum of Fig. 11 . We scan the relative branching ratios, assuming that no other decay mode is allowed. The largest excluded cross section (that is, to the worst upper limit) is found for each top-squark and neutralino mass. A branching-ratio independent limit is derived by comparing the worst-case exclusion to the corresponding top-squark pair production cross section. Unlike other other simplified model interpretations, this interpretation is not based on a specific choice of branching ratios. While a residual model dependence is introduced when only two decay modes are considered, this result is more generic than previous constraints.

# 9 Conclusion

We carried out a search for supersymmetric particles using proton-proton collision data collected by CMS at $\sqrt{s} = 8$ TeV. The dataset size corresponds to an integrated luminosity of 19.3 $fb^{-1}$. We analyzed events with at least two jets, at least one of which is identified as a b-tagged jet, and study the event distribution in the razor variables ($M_R$, $R^2$). The data were classified according to the muon, electron, jet, and b-tagged jet multiplicities. No significant excess was observed over the standard model background expectations, derived from a fit to

the data distribution in low-$M_R$ and low-$R^2$ sidebands.

The inclusive razor search was translated into the 95% confidence level exclusion limit on the masses of gluino and top squark, in the context of simplified natural SUSY models. For a neutralino mass of 100 GeV and depending on the branching ratios, the pair production of gluinos and top squarks in multi-bottom, multi-top, and mixed top-plus-bottom topologies was excluded for gluino masses up to 1375 GeV and squark masses up to 680 GeV. Using the combined likelihood of the hadronic boxes of the razor search and the single-lepton channels of the exclusive single lepton top-squark search, the exclusion bound on the top-squark mass was extended to 750 GeV (680 GeV) for a branching ratio $BR(\tilde{t} \to t\tilde{\chi}_1^0) = 100\%$ (50%) and a neutralino mass of 100 GeV. For the same neutralino mass, top squarks decaying to the two considered final states were excluded at 95% confidence level for masses larger than 380 GeV and smaller than 675 GeV, independent of the branching ratios.

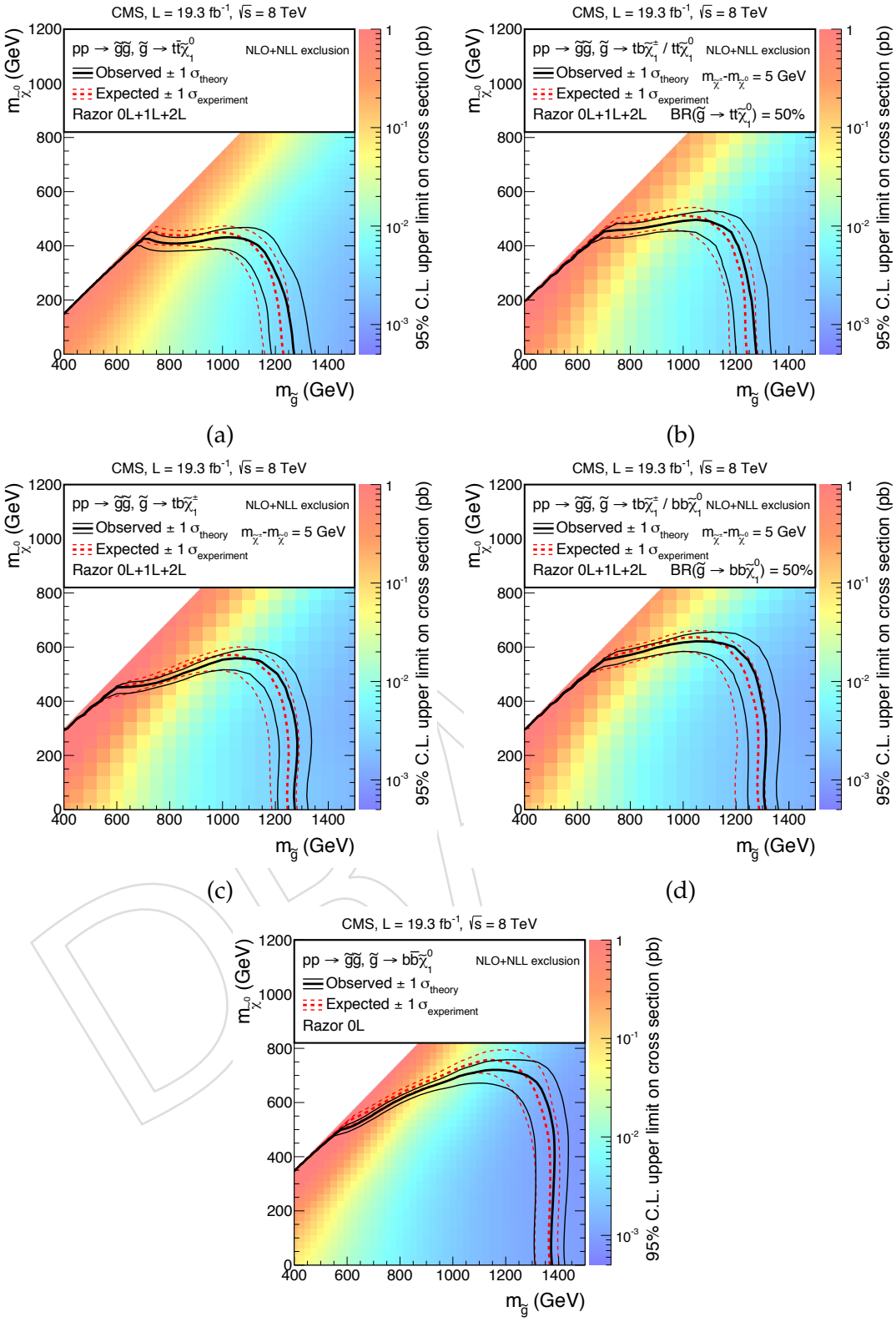


Figure 14: Interpretation of the inclusive search with razor variables in the context of gluino-mediated models: (a) T1tttt, (b) T1tttb, (c) T1ttbb, (d) T1tbbb, and (e) T1bbbb. The color coding denotes the observed 95% CL upper limit on the signal cross section. The dashed and solid lines represent the expected and observed exclusion contours at 95% CL, respectively. The dashed contours around the expected limit and the solid contours around the observed one represent the impact of the theoretical uncertainty in the cross section and the combination of the statistical and experimental systematic uncertainties, respectively.

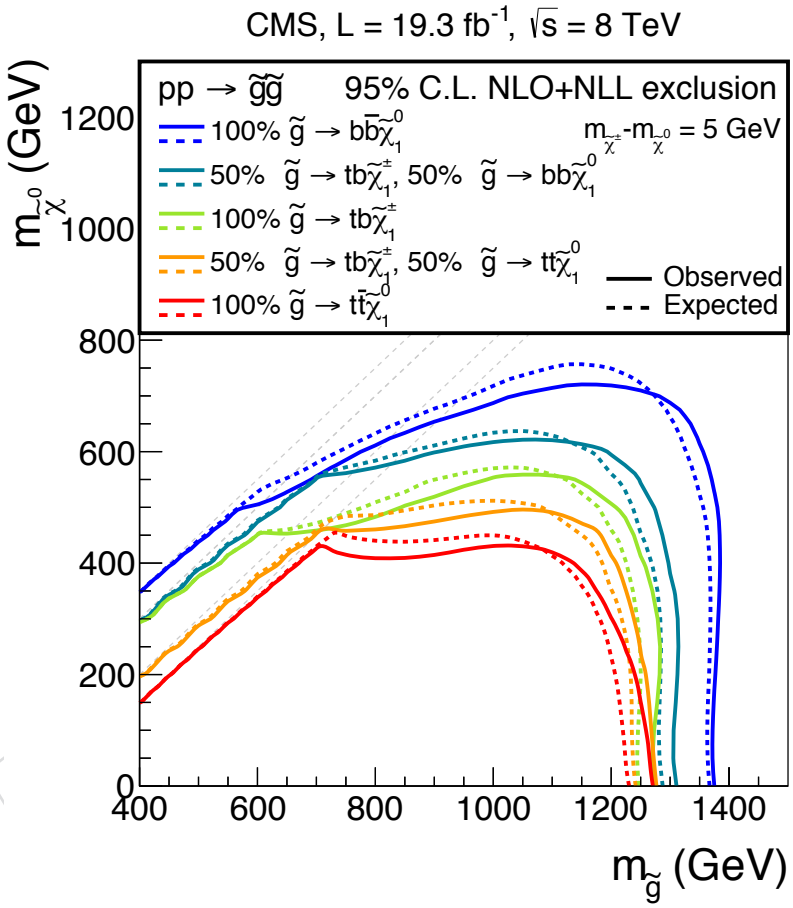


Figure 15: Gluino mass limit at 95% CL, obtained for different gluino-gluino models, using the nine boxes of the razor search, in the context of the benchmark natural SUSY spectrum of Fig. 11.

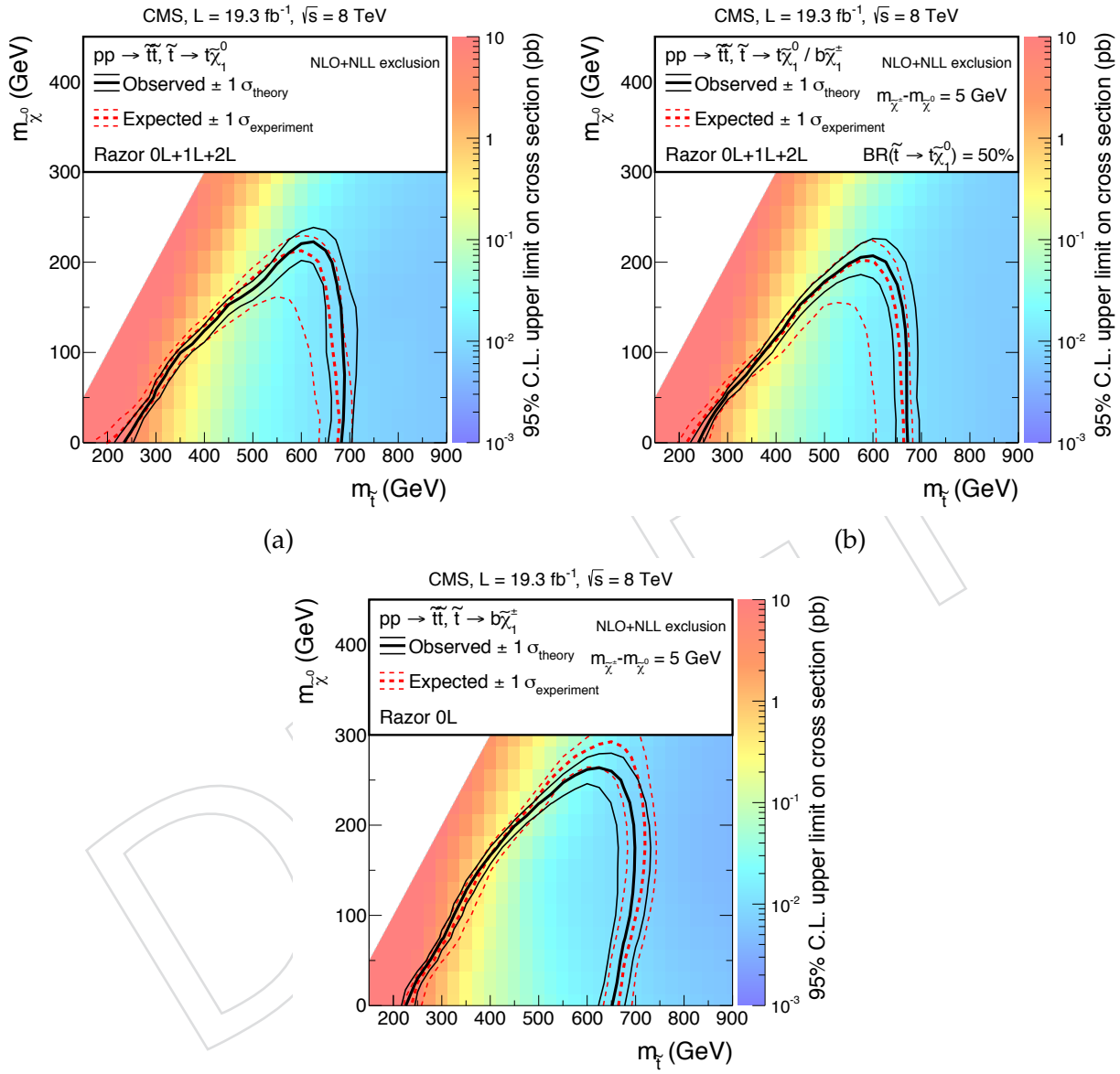


Figure 16: Interpretation of the inclusive search with razor variables in the context of top-squark-mediated models: (a) T2tt, (b) T2tb, and (c) T2bW*. The meaning of the color coding and the displayed contours are explained in the caption of Fig. 14.

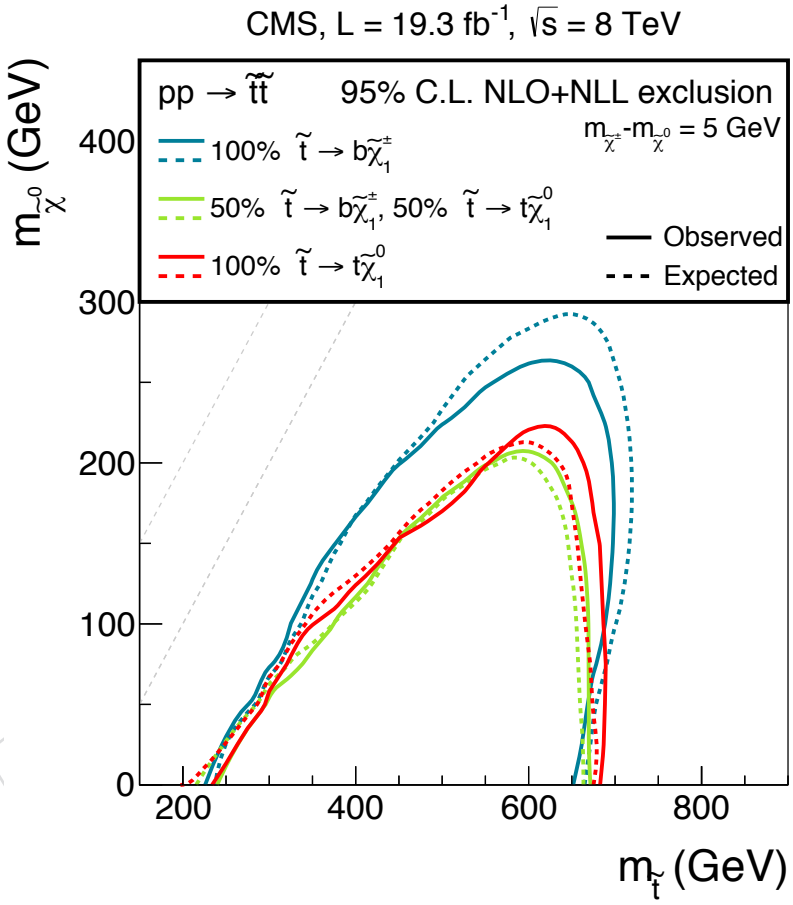


Figure 17: Top-squark mass limit at 95% CL, obtained for different squark-squark models with the inclusive razor analysis in the context of the benchmark natural SUSY spectrum of Fig. 11.

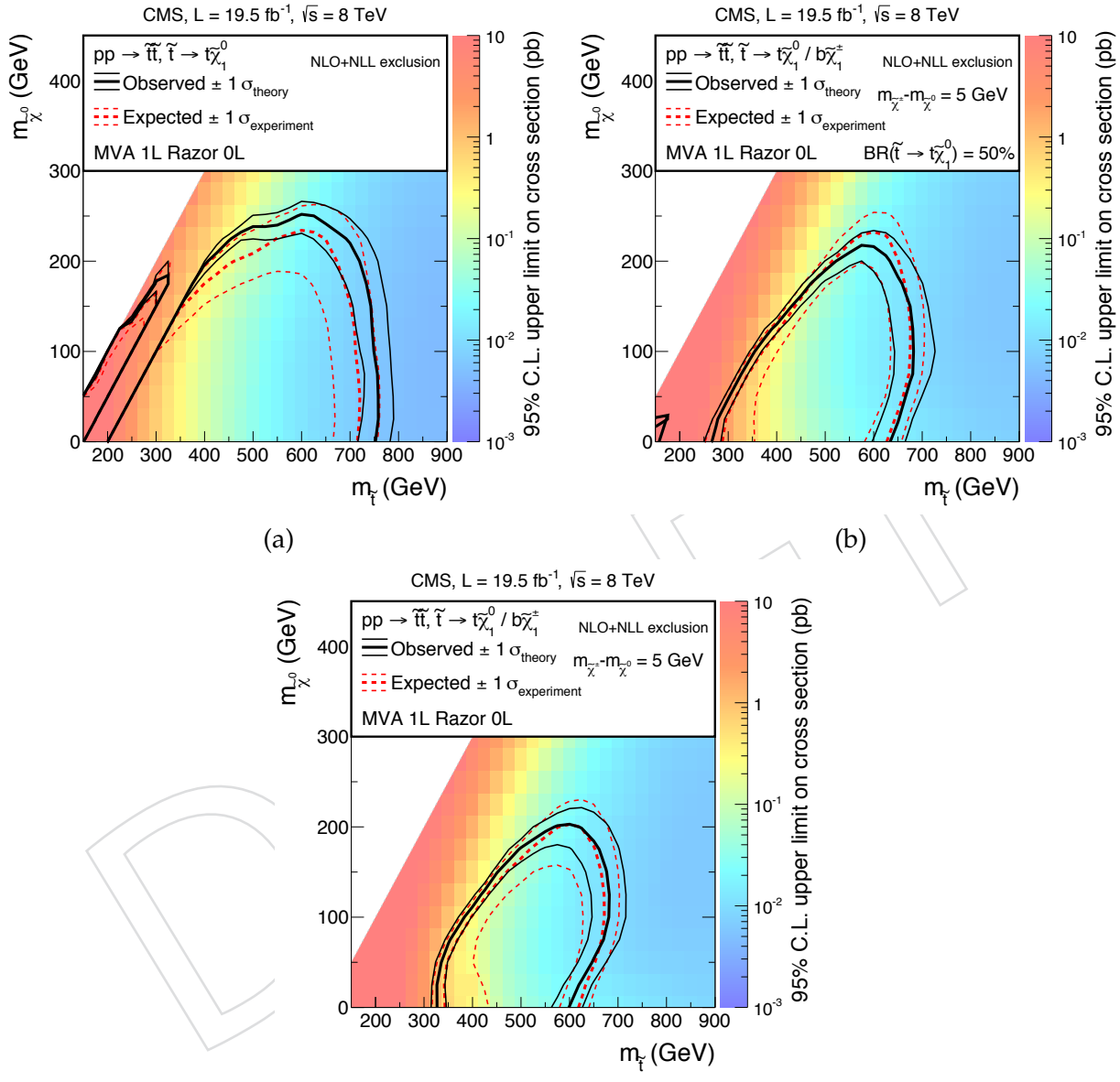


Figure 18: Top-squark mass limit at 95% CL, obtained combining the result of the hadronic razor boxes with the result of Ref. [28] for (a) T2tt, (b) T2tb, and (c) independent of the branching ratio choice.

# References


[1] J. Wess and B. Zumino, "Supergauge transformations in four-dimensions", *Nucl. Phys. B* **70** (1974) 39, doi:10.1016/0550-3213(74)90355-1.

[2] Y. A. Golfand and E. P. Likhtman, "Extension of the algebra of poincare group generators and violation of p invariance", *JETP Lett.* **13** (1971) 323.

[3] D. V. Volkov and V. P. Akulov, "Possible universal neutrino interaction", *JETP Lett.* **16** (1972) 438.

[4] A. H. Chamseddine, R. L. Arnowitt, and P. Nath, "Locally supersymmetric grand unification", *Phys. Rev. Lett.* **49** (1982) 970, doi:10.1103/PhysRevLett.49.970.

[5] G. L. Kane, C. F. Kolda, L. Roszkowski, and J. D. Wells, "Study of constrained minimal supersymmetry", *Phys. Rev. D* **49** (1994) 6173, doi:10.1103/PhysRevD.49.6173, arXiv:hep-ph/9312272.

[6] P. Fayet, "Supergauge invariant extension of the Higgs mechanism and a model for the electron and its neutrino", *Nucl. Phys. B* **90** (1975) 104, doi:10.1016/0550-3213(75)90636-7.

[7] R. Barbieri, S. Ferrara, and C. A. Savoy, "Gauge models with spontaneously broken local supersymmetry", *Phys. Lett. B* **119** (1982) 343, doi:10.1016/0370-2693(82)90685-2.

[8] L. J. Hall, J. D. Lykken, and S. Weinberg, "Supergravity as the messenger of supersymmetry breaking", *Phys. Rev. D* **27** (1983) 2359, doi:10.1103/PhysRevD.27.2359.

[9] P. Ramond, "Dual theory for free fermions", *Phys. Rev. D* **3** (1971) 2415, doi:10.1103/PhysRevD.3.2415.

[10] ATLAS Collaboration, "Observation of a new particle in the search for the Standard Model Higgs boson with the ATLAS detector at the LHC", *Phys. Lett. B* **716** (2012) 1, doi:10.1016/j.physletb.2012.08.020, arXiv:1207.7214.

[11] CMS Collaboration Collaboration, "Observation of a new boson at a mass of 125 GeV with the CMS experiment at the LHC", *Phys. Lett. B* **716** (2012) 30, doi:10.1016/j.physletb.2012.08.021, arXiv:1207.7235.

[12] M. Papucci, J. T. Ruderman, and A. Weiler, "Natural SUSY Endures", *JHEP* **1209** (2012) 035, doi:10.1007/JHEP09(2012)035, arXiv:1110.6926.

[13] CMS Collaboration, "Interpretation of Searches for Supersymmetry with simplified Models", *Phys. Rev. D* **88** (2013) 052017, doi:10.1103/PhysRevD.88.052017, arXiv:1301.2175.

[14] ATLAS Collaboration Collaboration, "Search for squarks and gluinos with the ATLAS detector in final states with jets and missing transverse momentum using 4.7 $\text{fb}^{-1}$ of $\sqrt{s} = 7$ TeV proton-proton collision data", *Phys.Rev.* **D87** (2013) 012008, doi:10.1103/PhysRevD.87.012008, arXiv:1208.0949.

[15] ATLAS Collaboration Collaboration, "Search for top and bottom squarks from gluino pair production in final states with missing transverse energy and at least three b-jets with the ATLAS detector", *Eur.Phys.J.* **C72** (2012) 2174, doi:10.1140/epjc/s10052-012-2174-z, arXiv:1207.4686.

[16] C. Rogan, "Kinematics for new dynamics at the LHC", (2010). arXiv:1006.2727. CALT-68-2790.

[17] CMS Collaboration, "Inclusive search for squarks and gluinos in pp collisions at $\sqrt{s} = 7$ TeV", *Phys. Rev. D* **85** (2012) 012004, doi:10.1103/PhysRevD.85.012004, arXiv:1107.1279.

[18] CMS Collaboration, "Inclusive search for supersymmetry using the razor variables in pp collisions at $\sqrt{s} = 7$ TeV", *Phys. Rev. Lett.* **111** (2013) 081802, doi:10.1103/PhysRevLett.111.081802, arXiv:1212.6961.

[19] CMS Collaboration, "Search for supersymmetry with razor variables in pp collisions at $\sqrt{s} = 7$ TeV", arXiv:1405.3961.

[20] ATLAS Collaboration Collaboration, "Multi-channel search for squarks and gluinos in $\sqrt{s} = 7$ TeV $pp$ collisions with the ATLAS detector", *Eur.Phys.J.* **C73** (2013) 2362, doi:10.1140/epjc/s10052-013-2362-5, arXiv:1212.6149.

[21] "Search for strongly produced supersymmetric particles in decays with two leptons at $\sqrt{s}$ = 8 TeV", Technical Report ATLAS-CONF-2013-089, CERN, Geneva, (Aug, 2013).

[22] N. Arkani-Hamed et al., "MARMOSET: The path from LHC data to the new standard model via on-shell effective theories", (2007). arXiv:hep-ph/0703088.

[23] J. Alwall, P. Schuster, and N. Toro, "Simplified models for a first characterization of new physics at the LHC", *Phys. Rev. D* **79** (2009) 075020, doi:10.1103/PhysRevD.79.075020, arXiv:0810.3921.

[24] J. Alwall, M.-P. Le, M. Lisanti, and J. G. Wacker, "Model independent jets plus missing energy searches", *Phys. Rev. D* **79** (2009) 015005, doi:10.1103/PhysRevD.79.015005, arXiv:0809.3264.

[25] D. S. Alves, E. Izaguirre, and J. G. Wacker, "Where the sidewalk ends: jets and missing energy search strategies for the 7 TeV LHC", *JHEP* **10** (2011) 012, doi:10.1007/JHEP10(2011)012, arXiv:1102.5338.

[26] LHC New Physics Working Group Collaboration, "Simplified models for LHC new physics searches", *J. Phys. G* **39** (2012) 105005, doi:10.1088/0954-3899/39/10/105005, arXiv:1105.2838.

[27] CMS and ATLAS Collaboration, "Procedure for the LHC Higgs boson search combination in Summer 2011", Technical Report CMS-NOTE-2011-005, CERN, Geneva, (Aug, 2011).

[28] CMS Collaboration Collaboration, "Search for top-squark pair production in the single-lepton final state in pp collisions at $\sqrt{s}$ = 8 TeV", *Eur.Phys.J.* **C73** (2013) 2677, doi:10.1140/epjc/s10052-013-2677-2, arXiv:1308.1586.

[29] CMS Collaboration, "The CMS experiment at the CERN LHC", *JINST* **3** (2008) S08004, doi:10.1088/1748-0221/3/08/S08004.

[30] CMS Collaboration, "Particle–flow event reconstruction in CMS and performance for jets, taus, and $E_{\mathrm{T}}^{\mathrm{miss}}$", CMS Physics Analysis Summary CMS-PAS-PFT-09-001, (2009).

[31] CMS Collaboration, "Commissioning of the particle-flow event reconstruction with the first LHC collisions recorded in the CMS detector", CMS Physics Analysis Summary CMS-PAS-PFT-10-011, (2010).

[32] M. Cacciari, G. P. Salam, and G. Soyez, "The catchment area of jets", *JHEP* **04** (2008) 005, doi:10.1088/1126-6708/2008/04/005, arXiv:0802.1188.

[33] M. Cacciari and G. P. Salam, "Pileup subtraction using jet areas", *Phys. Lett. B* **659** (2008) 119, doi:10.1016/j.physletb.2007.09.077, arXiv:0707.1378.

[34] CMS, "Determination of jet energy calibration and transverse momentum resolution in CMS", *JINST* **6** (2011) P11002, doi:10.1088/1748-0221/6/11/P11002, arXiv:1107.4277.

[35] M. Cacciari, G. P. Salam, and G. Soyez, "FastJet User Manual", *Eur. Phys. J. C* **72** (2012) 1896, doi:10.1140/epjc/s10052-012-1896-2, arXiv:1111.6097.

[36] M. Cacciari, G. P. Salam, and G. Soyez, "The anti-$k_{\mathrm{T}}$ jet clustering algorithm", *JHEP* **04** (2008) 063, doi:10.1088/1126-6708/2008/04/063, arXiv:0802.1189.

[37] CMS Collaboration, "Performance of b tagging at $\sqrt{s} = 8$ TeV in multijet, $\mathrm{t\bar{t}}$ and boosted topology events", technical report, (2013).

[38] J. Alwall et al., "MadGraph5 : going beyond", *JHEP* **06** (2011) 128, doi:10.1007/JHEP06(2011)128, arXiv:1106.0522.

[39] J. Alwall et al., "The automated computation of tree-level and next-to-leading order differential cross sections, and their matching to parton shower simulations", doi:10.1007/JHEP07(2014)079, arXiv:1405.0301.

[40] T. Sjöstrand, S. Mrenna, and P. Skands, "PYTHIA 6.4 physics and manual", *JHEP* **05** (2006) 026, doi:10.1088/1126-6708/2006/05/026, arXiv:hep-ph/0603175.

[41] S. Hoeche et al., "Matching parton showers and matrix elements", (2006). arXiv:hep-ph/0602031.

[42] GEANT4 Collaboration, "GEANT4: a simulation toolkit", *Nucl. Instrum. Meth. A* **506** (2003) 250–303, doi:10.1016/S0168-9002(03)01368-8.

[43] W. Verkerke and D. P. Kirkby, "The RooFit toolkit for data modeling", *eConf* **C0303241** (2003) MOLT007, arXiv:physics/0306116.

[44] CMS Collaboration, "The fast simulation of the CMS detector at LHC", *J. Phys. Conf. Ser.* **331** (2011) 032049, doi:10.1088/1742-6596/331/3/032049.

[45] W. Beenakker, R. Höpker, M. Spira, and P. M. Zerwas, "Squark and gluino production at hadron colliders", *Nucl. Phys. B* **492** (1997) 51, doi:10.1016/S0550-3213(97)80027-2, arXiv:hep-ph/9610490.

[46] A. Kulesza and L. Motyka, "Threshold resummation for squark-antisquark and gluino-pair production at the LHC", *Phys. Rev. Lett.* **102** (2009) 111802, doi:10.1103/PhysRevLett.102.111802, arXiv:0807.2405.

[47] A. Kulesza and L. Motyka, "Soft gluon resummation for the production of gluino-gluino and squark-antisquark pairs at the LHC", *Phys. Rev. D* **80** (2009) 095004, doi:10.1103/PhysRevD.80.095004, arXiv:0905.4749.

[48] W. Beenakker et al., "Soft-gluon resummation for squark and gluino hadroproduction", *JHEP* **12** (2009) 041, doi:10.1088/1126-6708/2009/12/041, arXiv:0909.4418.

[49] W. Beenakker et al., "Squark and gluino hadroproduction", *Int.J.Mod.Phys. A* **26** (2011) 2637, doi:10.1142/S0217751X11053560, arXiv:1105.1110.

[50] M. Krämer et al., "Supersymmetry production cross sections in pp collisions at $\sqrt{s} = 7$ TeV", (2012). arXiv:1206.2892.

[51] D. Bourilkov, R. C. Group, and M. R. Whalley, "LHAPDF: PDF use from the Tevatron to the LHC", (2006). arXiv:hep-ph/0605240.

[52] S. Alekhin et al., "The PDF4LHC Working Group Interim Report", (2011). arXiv:1101.0536.

[53] M. Botje et al., "The PDF4LHC Working Group Interim Recommendations", (2011). arXiv:1101.0538.